AIAA JOURNAL
Vol. 47, No. 9, September 2009

Aerodynamic Stall Suppression on Airfoil Sections Using Passive Air-Jet Vortex Generators

S. A. Prince,* V. Khodagolian,† and C. Singh†
City University, London, England EC1V 0HB, United Kingdom
and
T. Kokkalis‡
CeBeNetwork, GmbH, 28199 Neustadt, Bremen, Germany

DOI: 10.2514/1.41986

This paper presents an experimental and computational study of a passive version of the air-jet vortex-generator flow control system for the delay or suppression of trailing-edge boundary-layer separation and subsequent stall. The results show that a passive vortex-generating jet flow control system, which uses the high pressure from the leading-edge attachment line to feed the upper-surface air jets, can effectively delay trailing-edge separation and subsequent stall to higher angles of attack, without the need for any active energy input and without significant drag penalty.

Nomenclature

C_A	=	axial force coefficient
C_D	=	drag force coefficient
C_L	=	lift force coefficient
C_M	=	quarter-chord pitching moment coefficient
C_p	=	pressure coefficient
C_μ	=	blowing momentum coefficient
c	=	chord length, m
$\dot{m}$	=	mass flow rate through the air-jet vortex-generator duct, kg/s
p	=	static pressure, N/m^2
S	=	reference, model planform) area, m^2
U	=	velocity, m/s
x	=	chordwise distance from leading-edge, m
y	=	spanwise distance from model center, m
z	=	distance normal to the chord line, m
α	=	angle of attack, deg
ρ	=	density, kg/m^3
ϕ	=	air-jet pitch angle, deg
ψ	=	air-jet skew angle, deg

Subscripts

j	=	average conditions in jet at exit
t	=	conditions at trailing edge
∞	=	freestream conditions

I. Introduction

VARIOUS flow control techniques to reenergize boundary layers and thereby suppress flow separation have been successfully tested, such as slot blowing, tangential blowing, and synthetic jets. The method of increasing fluid mixing rates by the artificial generation of near-surface streamwise vortices has been found to be a particularly powerful technique. The vortices act to entrain high-energy flow from the undisturbed outer airstream and transport it into the low-momentum near-wall region deep inside the boundary layer. Mechanical passive vane vortex generators, first devised by Taylor and Hoadley [1], are the most common and widely used streamwise fluid vortex generators and commonly consist of thin solid strips fixed to the surface. However, it has been shown that vane vortex generators impose an increase in drag, caused by both the local pressure increase derived from the flow blockage by the device itself and by an increase in surface skin friction downstream in the device wake.

An alternative to vane vortex generators is an active fluid jet vortex generator, proposed by Wallis [2]. Fluid injection via inclined and skewed (relative to the freestream flow) wall-bounded jets act to induce longitudinal vortices for flow control, instead of solid vane vortex generators. Air-jet vortex generators (AJVGs) usually consist of an array of small orifices embedded in a surface and supplied by a pressurized air source, wherein longitudinal vortices are induced by the interaction between the jets issuing from each orifice and a freestream fluid flow, as shown in Fig. 1. The orifices are pitched at angle ϕ with respect to the surface tangent and skewed at angle ψ with respect to the freestream flow.

Air-jet vortex generators, unlike passive vane vortex generators, do not induce a large increase in drag and they can be actively operated and controlled. Following the work of Wallis [2], Pearcey [3] undertook a considerable series of experimental studies demonstrating the effectiveness of AJVGs for low- and high-speed flows. Freestone [4] performed a study of both vane vortex generators and AJVGs (with both circular and rectangular jet orifices) at low speeds and identified that the optimum jet orientation for maximum vorticity generation was a pitch angle (relative to the local surface tangent) of 30 deg and a skew angle (relative to the freestream flow vector) of 60 deg. With this orientation, Freestone showed that the resulting vortex strength could match and, in some cases, exceed that generated by an equivalent vane vortex generator. Many further studies [5–12] have been performed over the years into the application of active vortex-generating jets for stall suppression. The major detriment, however, to the application of active air-jet blowing flow control is its requirement for active energy input: electrical energy for compressing and pumping high-pressure air, for example. In addition, the system must be supplied from a source such as the engine in which intake air can be bled away to feed the jets. In this case, the system will then result in a small loss in engine efficiency, equivalent to an increase in parasitic drag.

This study presents an experimental and computational assessment of a passive version of the air-jet vortex generator in which the internal plenum chamber is removed and the individual upper-surface jet orifices connected to the lower-surface leading edge by a tube, such that feed air is supplied by ram air induction from the high-

Received 4 November 2008; revision received 22 April 2009; accepted for publication 26 April 2009.

*Senior Lecturer, Centre for Aeronautics. Member AIAA.
†Research Assistant, Centre for Aeronautics.
‡Consultant Engineer, Flight Physics Department.

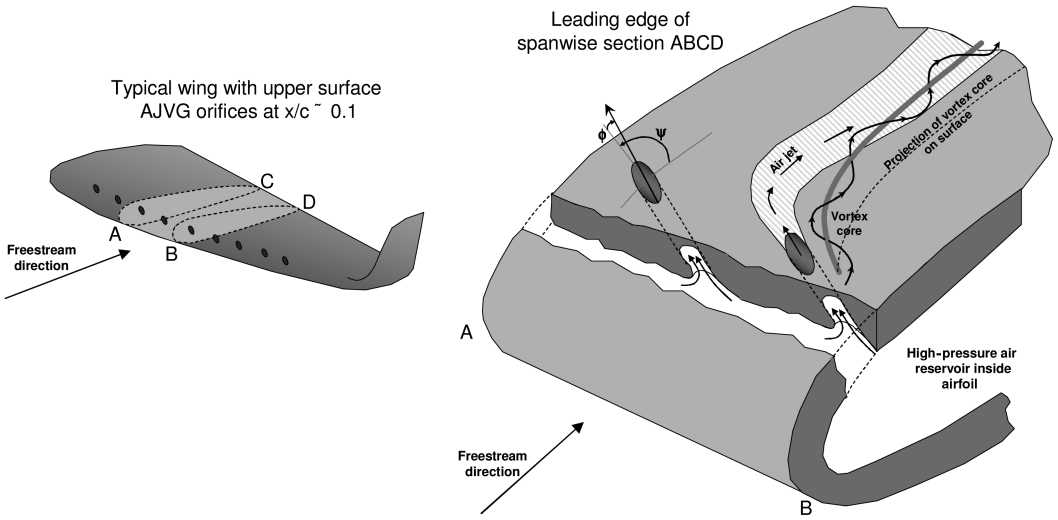

Fig. 1 Typical geometry of a leading-edge array of air-jet vortex generators with illustration of the physics of longitudinal vortex formation [3].

pressure region in the vicinity of the attachment line. This system could be employed for the same applications as active air-jet systems are currently being investigated, for instance, in conjunction (but not replacing) high-lift slats and flaps. The basic concept derives from the work of Oliver [9] and Raghunathan et al. [10] and was developed and tested by Singh and Prince [13], Prince [14], and Prince et al. [15] as part of a U.K. national study on technologies for next-generation helicopter rotor systems between 2002–2008. An independent study of this concept has also recently been reported by Krzysiak [16].

II. Experimental Study

Two airfoil-section models were designed and constructed to experimentally measure the effect of a passive AJVG system located at 12% chord. An airfoil of moderate thickness-to-chord ratio was chosen as well as a much thicker section to better test the effectiveness of the passive AJVG to suppress static stall across the range of airfoil thickness-to-chord ratio. The first model employed the NACA 23012C airfoil section: a modification of the NACA 23012 section, with increased camber and a modified trailing edge to promote trailing-edge separation [17]. The model was initially designed with an active AJVG system fed by an internal plenum pipe with compressed air blown in at either end. The model, with a chord of 481 mm and a span of 740 mm, was fitted with a spanwise array of 15 air jets of 4.8-mm-diam circular orifices, located at 12% chord and spaced equally apart at 45 mm between jet centers. In addition, the model was fitted with large end plates to enforce quasi-2-D flow and with leading-edge sand-roughness transition strips. The air-jet orifices were designed with 30 deg pitch angle and 60 deg skew angle to the local airfoil surface and freestream flow direction.

Once the active blowing experiments were completed, the model was then modified by removing the internal plenum tube and connecting the upper-surface AJVG orifices via a curved 4.8-mm-diam steel tube to contoured intakes (employing 3 mm corner rounding) at 4% chord on the lower surface. Smoothly contoured intakes are necessary to ensure that a smooth undistorted flow is induced into the duct by preventing any intake separation. This also ensures high levels of intake mass flow and limits the disturbances that feed into the lower-surface boundary layer.

With the limited space available within the leading-edge region of the airfoil, it was not possible to achieve the correct positioning of the intake and exit orifice without a considerable curvature of the duct pipe, which would almost certainly lead to internal flow separation and the generation of considerable swirl. Figure 2 shows the level of duct curvature that was needed to ensure that the intake duct was situated at $x/c = 0.04$, and the duct exit was at a location $x/c = 0.12$ for the cases of 30 deg skew (computation only) and 60 deg skew angles, both with 30 deg pitch angle.

A second model, with a greater thickness-to-chord ratio, incorporating a NACA 63_2-217 section, was constructed with an

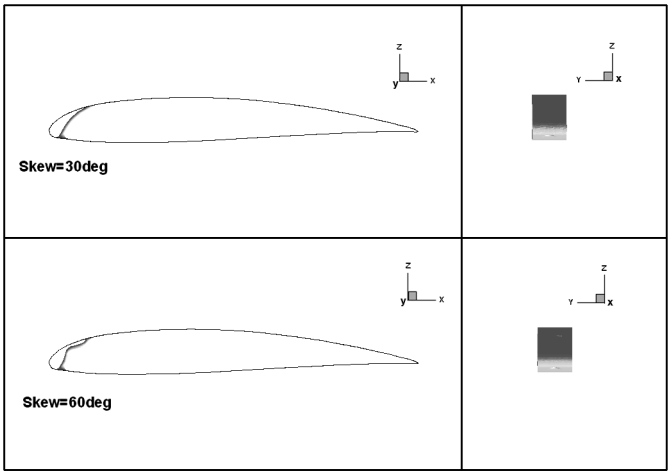

a) AJVG arrangement, with bent tube ducts

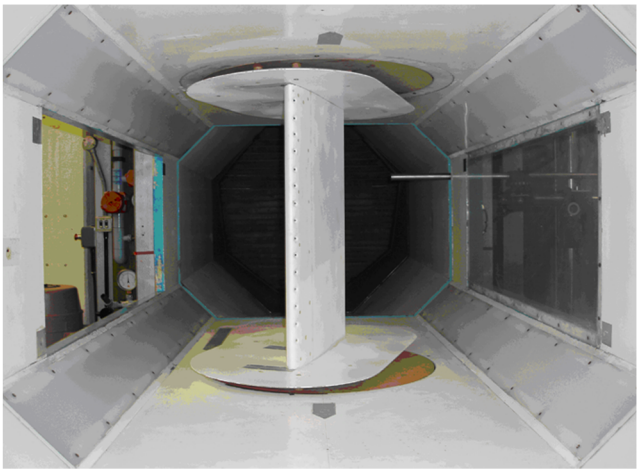

a) Model with passive AJVG in T2 wind tunnel

Fig. 2 Details of the NACA 23012C airfoil model.

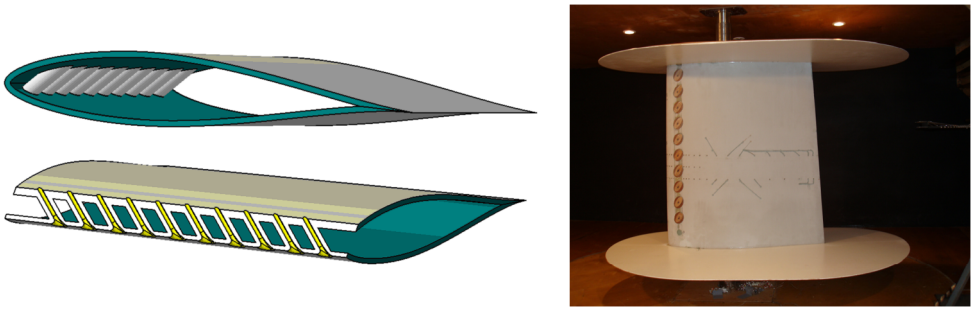

a) General configuration and cutaway view b) Model in the industrial wind tunnel

Fig. 3 NACA 63_2-217 airfoil-section model with spanwise array of 10 straight passive AJVGs installed.

array of 10 passive AJVGs, as shown in Fig. 2. The model was of span 975 mm and 800 mm chord, and the AJVGs orifices (10 mm diameter) were located at 12% chord with 84 mm spanwise separation between the intake orifice centers. Both models employed the same percentage chordwise location and local pitch and skew angles, which were chosen based on the optimum values identified by Freestone [4]. For this second model, there was enough space to allow straight ducts, as shown in Fig. 3, such that flow separation and swirl were minimized.

Both models were instrumented with three chordwise lines of 82 static pressure orifices each, to allow the measurement of the surface pressure distributions on chordwise planes passing through 1) the center of the orifice located on the centerline of the model, 2) the plane halfway between this orifice and its adjacent orifice, and 3) another plane in the middle of these two. The pressure tappings were constructed from a 0.5-mm-i.d. brass tube embedded flush with the surface of the model. One of the tappings in each array was located at the trailing edge, such that trailing-edge pressure could be monitored.

The momentum deficit through the wake one chord length downstream of the trailing edge was measured using a wake rake. The wake rake consisted of 40 stainless steel pitot probes and 5 static probes (o.d. of 1.05 mm and i.d. of 0.81 mm). The pitot pressure probes were spaced at 7 mm intervals in the center and at 15 mm intervals toward each spanwise extremity, giving a total span of 350 mm. The static pressure tubes were used to measure any static pressure gradient across the wake. Measuring the pitot and static pressures through the wake permits the calculation of the drag coefficient using the Jones [18] method.

A 48-probe shear-layer rake was also employed to measure the spanwise distribution of dynamic pressure through the upper-surface boundary layer at a number of chordwise planes during the NACA 23012C series of experiments. The pressures were recorded using a piezosensitive pressure measurement system from Chell System. The accuracy of these pressure measurements is estimated to be $\Delta C_p = \pm 0.02$ at 35 m/s freestream speed and ± 0.05 at 25 m/s freestream speed. Spanwise-averaged surface pressure distributions were then used, via an integration routine, to calculate the normal force coefficient C_N, the axial force coefficient C_A, and the pitching moment coefficient referenced to the quarter-chord axis C_M. From previous tests using a similar density and distribution of pressure orifices, which were compared with simultaneous force and moment measurements from a six-component strain-gauge balance, the integrated normal force and pitching moments were found to be within 5% of the measured results at 0 deg angle of attack, reducing to about 1% at high angle of attack.

The NACA 23012C experiments were performed in the City University T2 low-speed wind tunnel at speeds in the range of 15–35 m/s ($0.7 \times 10^6 < Re_C < 1.1 \times 10^6$), and the NACA 63_2-217 experiments were performed in the City University industrial wind tunnel in the speed range of 5–25 m/s ($0.27 \times 10^6 < Re_C < 1.3 \times 10^6$). The models were continuously pitched in angle of attack and the working-section dynamic pressure was maintained constant. Maximum blockage was estimated at 14% for the highest angle of attack of $\alpha = 30$ deg. Accuracy of the geometric angle-of-attack measurements has been estimated at ± 0.5 deg.

III. Computational Study of the NACA 23012C Airfoil Model Case

A computational fluid dynamics (CFD) study was also performed for both the NACA 23012C and NACA 63_2-217 cases. A commercial 3-D time-marching Navier–Stokes (N-S) flow solver and grid generation package was used to predict aerodynamic characteristics within the 0–25 deg angle-of-attack range [19]. Three turbulence models were tested: the Spalart–Allmaras [20], the k-ε[21] [21], and the k-ω (SST) [22] turbulence models. In this paper the CFD results for the NACA 23012C baseline (clean surface) airfoil are presented across the pitch range, and for the passive AJVG case only the $\alpha = 0$ and 18 deg results are presented. The flows for the 30 and the 60-deg-skewed passive air-jet geometries were computed for these conditions. For the NACA 63_2-217 study, baseline and passive AJVG solutions were obtained for $\alpha = 0$ deg, 18 and 25 deg only.

The time-marching flow solver used in this study is based on the finite volume method and can use structured, unstructured or hybrid grids. The coupled solver, which simultaneously computes both the continuity, momentum and energy equations, was employed. The solver uses an upwind, flux-difference splitting algorithm and can operate using either implicit or explicit time-marching schemes. For the present investigation the spatial accuracy was set to second order.

The geometries and the flowfields were assumed to be periodically symmetric about any constant-y planes separated by a distance Δy (the spanwise separation between the centers of successive air-jet orifices). For the NACA 23012C case $\Delta y = 45$ mm, and for the NACA 63_2-217 case $\Delta y = 84$ mm. A computational model was

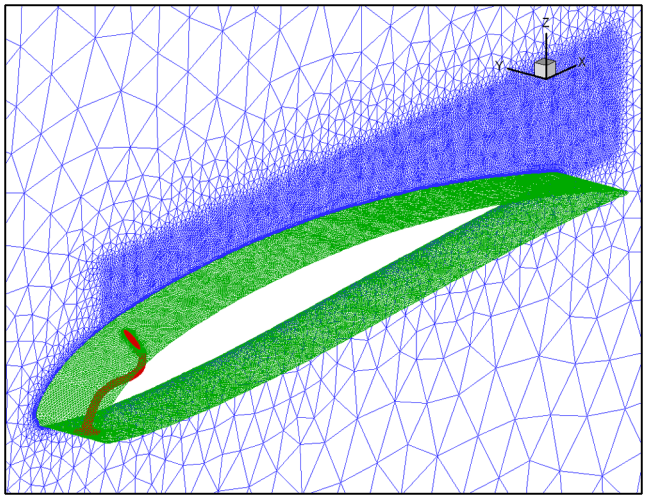

Fig. 4 NACA 23012C 1.7-million-cell single-element, computational grid for the 60-deg-skewed jet case. The airfoil surface grid, the air-jet duct surface grid, and the $y = 45$ mm periodic plane are plotted.

Table 1 Grid sizes for NACA 23012C model numerical study

Grid	Number of cells
1 coarsest	550,653
2	605,125
3	1,148,223
4	1,675,782
5 finest	2,161,927

therefore constructed of a 45 mm spanwise element, for the NACA 23012C case, and an 84 mm spanwise element for the NACA 63_2-217 case that fully encompassed a single air-jet intake-duct-orifice, as shown in Fig. 4 for the NACA 23012C model. This assumption is valid, based on the published literature, as long as the flow is steady and is attached over the majority of the upper-surface. A periodic boundary condition was applied, linking the flow solution on the two constant-y boundaries.

Five computational grids were employed for each study, to ensure grid convergence. A layer of 25 prismatic cells were embedded over the airfoil surface with the first cell height set at 1×10^{-6} chord lengths to resolve the boundary-layer characteristics with $1.0 < y^+ < 10.0$. Table 1 presents the grid size details for the 60-deg-skewed passive AJVG predictions for the NACA 23012C model study. A similar set of grid sizes were employed for the NACA 63_2-217 analysis.

IV. Results

A. Passive and Active AJVG Blowing on the NACA 23012C Model

The comparisons between the turbulent Navier–Stokes predicted and the experimentally derived variation of the aerodynamic

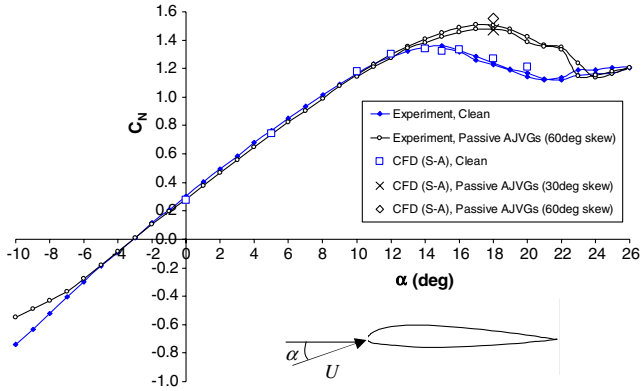

a) Normal force coefficient

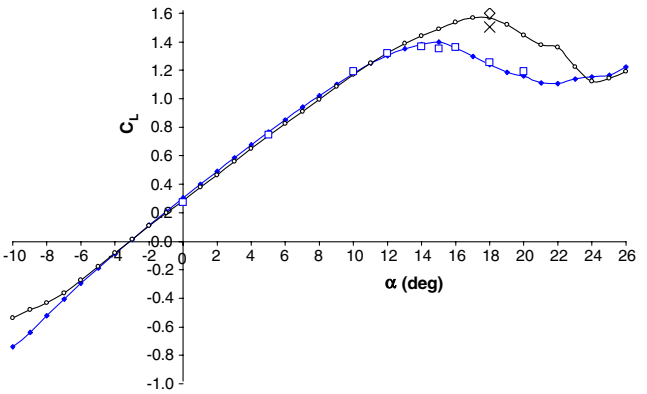

b) Lift coefficient

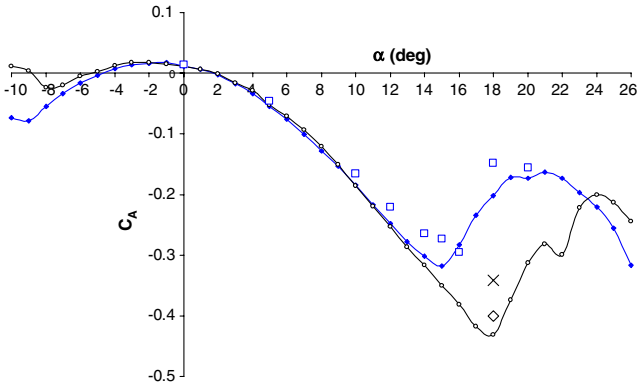

c) Axial force coefficient (neglecting skin friction)

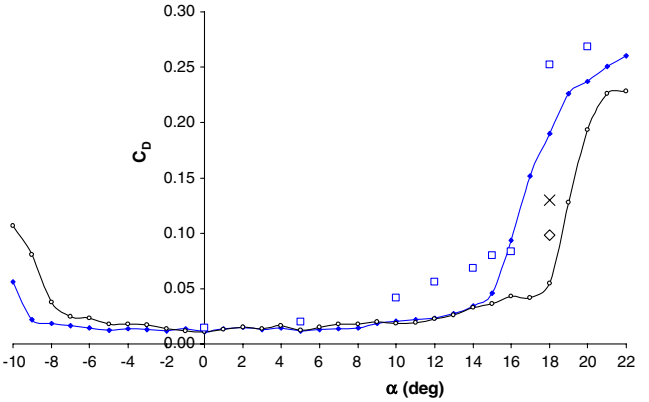

d) Drag coefficient (neglecting skin friction)

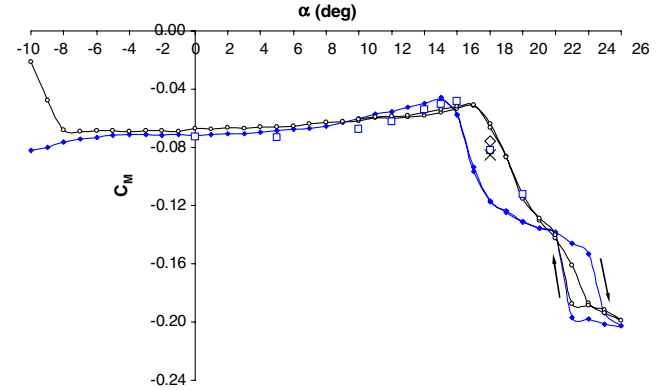

e) Quarter-chord pitching moment coefficient

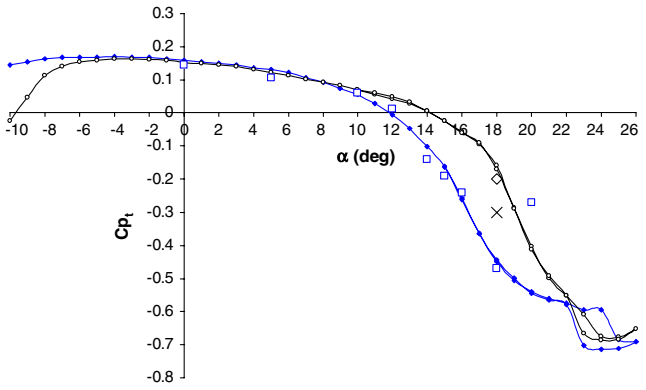

f) Trailing-edge pressure coefficient

Fig. 5 Variation with incidence of computed (N-S turbulent) and experimental aerodynamic characteristics for NACA 23012C model at $U = 35$ m/s and $Re_C = 1.1 \times 10^6$ (S-A denotes Spalart–Allmaras).

characteristics with angle of attack are presented in Fig. 5 for the case of $U = 35$ m/s. Figure 6 compares the CFD predicted contours of velocity magnitude through the upper-surface boundary layer with the corresponding experimental result at three chordwise locations.

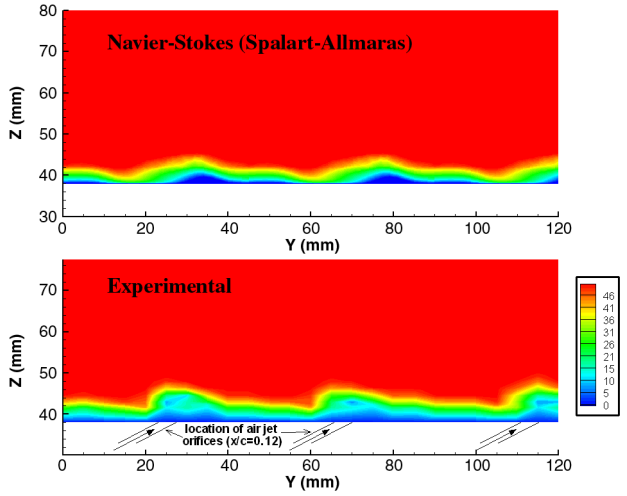

a) x/c = 0.2

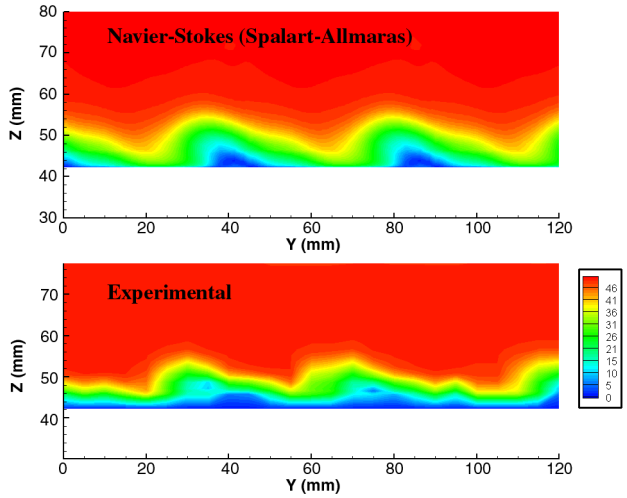

b) x/c = 0.3

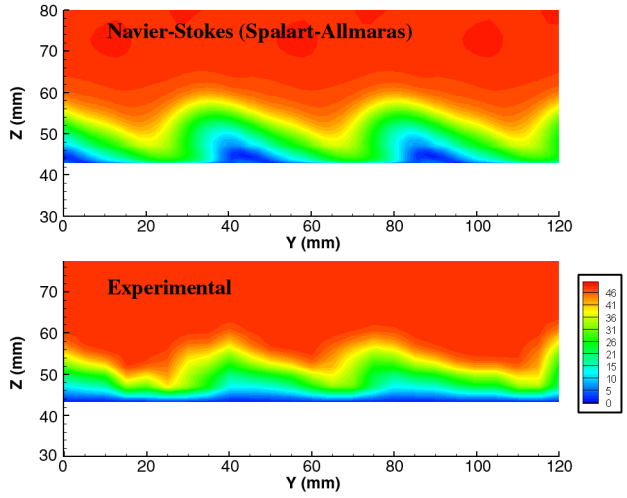

c) x/c = 0.4

Fig. 6 Comparison between CFD predicted and experimentally measured velocity magnitude contours (m/s) in the upper-surface boundary-layer/embedded longitudinal vortex, at three axial planes along the NACA 23012C model with passive air jets at $x/c = 0.12$, $U = 35$ m/s, and $Re_C = 1.1 \times 10^6$.

The computed velocity contours at the chordwise plane midway between the passive air-jet exits ($y = 0$ mm and 45 mm in the computational grid) and the chordwise plane through the jet exit centers are presented for $\alpha = 18$ deg, for the clean-airfoil and both passive AJVG cases, in Fig. 7.

Figure 8 then presents the comparisons of the CFD predicted and experimentally measured surface pressure distributions at the jet center and midjet spanwise locations, at $\alpha = 18$ deg for the clean-airfoil and the 60-deg-skewed passive AJVG cases. The CFD predictions were used to obtain an estimate of how the pressure difference (between the passive AJVG intake and exit) that drives the passive AJVG varies with angle of attack. This variation is plotted in Fig. 9.

The comparison between the aerodynamic performance of the passive and the active blowing (with C_μ of 0.01) AJVG systems on the NACA 23012C, undertaken in a separate set of experiments, are presented in Fig. 10. Note that the blowing momentum coefficient is defined as

$$C_\mu = \frac{\dot{m} U_j}{\frac{1}{2}\rho U_\infty^2 S}$$

where $\dot{m}$ is the mass flow rate of air passing through an air-jet duct (Pa), ρ is the freestream air density (kg/m^3), U_j is the average air-jet velocity exiting from the air-jet orifice (m/s), U_∞ is the freestream velocity (m/s), and S is the planform area of the model (m^2).

B. Passive AJVG Blowing on the NACA 63_2-217 Model

For the NACA 63_2-217 model a CFD study was undertaken, obtaining steady, turbulent (Spalart–Allmaras model only) Navier–Stokes solutions for the baseline airfoil and with the 60-deg-skewed passive AJVG array for $\alpha = 0$ deg, 18 and 25 deg. Figure 11 compares the variation of the measured and computed aerodynamic characteristics with angle of attack for the clean-airfoil and with the 60-deg-skewed passive air jets operating. Results of the wake traverse experiments, for the experimental calculation of drag, are compared in Table 2.

The computed velocity contours at the chordwise plane midway between the passive air-jet exits ($y = 0$ mm and 84 mm in the computational grid) and the chordwise plane through the jet exit centers are presented for $\alpha = 18$ and 25 deg, for the clean-airfoil and passive AJVG cases, in Fig. 12.

V. Discussion

A. Passive and Active AJVG Blowing on the NACA 23012C Model

The grid sensitivity study performed for the NACA 23012C study revealed that the force and moment predictions for the 1.67-million-cell passive air-jet grid and the corresponding 2.16-million-cell grid were equivalent to three significant figures, and the finest-grid result could then be regarded as a grid-independent solution.

Inspection of Fig. 5 shows that the turbulent N-S solutions for the baseline clean-airfoil model agreed remarkably well with the experimentally derived (integration of surface pressure) measurements. The CFD solutions successfully resolved the occurrence of trailing-edge separation ($C_{p_t} = 0$) at $\alpha \approx 12$ deg, and stall, indicated by C_N and C_A, at $\alpha \approx 15$–16 deg. The Spalart–Allmaras predictions resolved the magnitude of C_N to within 3% of the experimental measurement, which itself was estimated to be accurate to within 5% (based on the accuracy of the pressure measurement system and of the pressure integration algorithm). Although the agreement between the experimental and predicted axial force coefficients was not as good the turbulent N-S solutions successfully resolved the correct trends. This is as expected because the magnitude of the axial force is much smaller than the normal force, and the experimental pressure integration algorithm more sensitive to numerical error. The Spalart–Allmaras turbulence model predicted C_A magnitudes much closer to the experimental values than the k-ω shear stress transport (SST) model. Both turbulence models predicted the pitching moment to

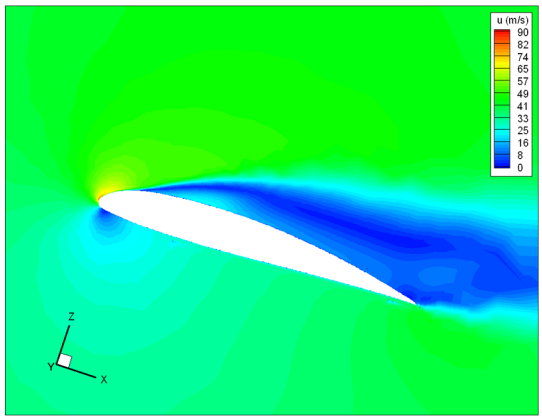

a) Clean airfoil

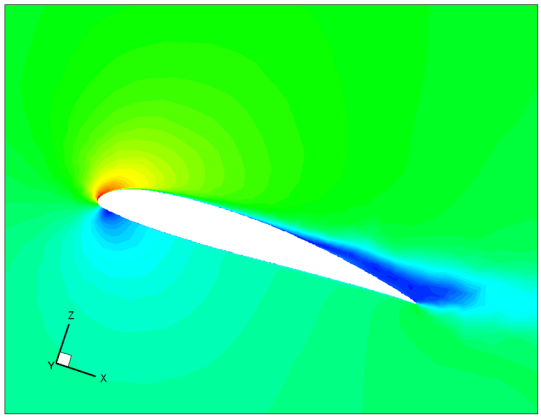

b) Passive air jets, 30 deg skew, midjet plane

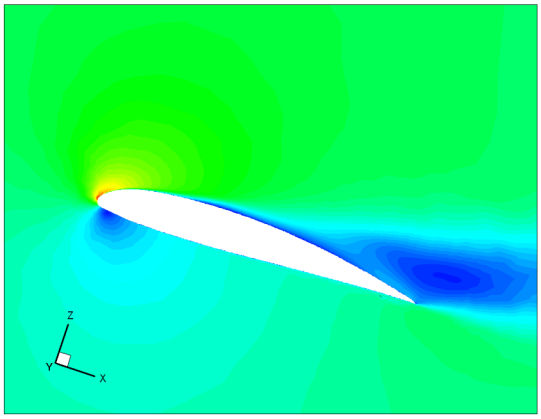

c) Passive air jets, 60 deg skew, midjet plane

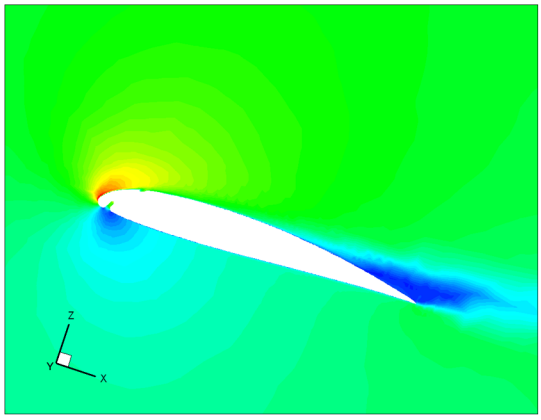

d) Passive air jets, 30 deg skew, jet exit center plane

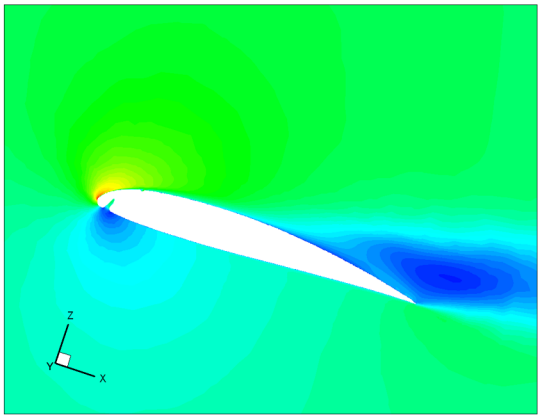

e) Passive air jets, 60 deg skew, jet exit center plane

Fig. 7 Comparison of computed velocity contours at spanwise slices midway between the passive air-jet exit centers and through the passive air jet center, for the NACA 23012C 0 cases of 30 and 60 deg air-jet skew and the corresponding clean-airfoil case; $U = 35$ m/s, $\alpha = 18$ deg, and $Re_C = 1.1 \times 10^6$.

within 5% of the experimental values in the prestall angle-of-attack range.

CFD results for the PAJVG cases are plotted for $\alpha = 0$ and 18 deg for the Spalart–Allmaras results only, because these were found to be marginally better than those obtained with the other turbulence models. At $\alpha = 0$ deg, it should be noted that both the experimental measurements and the CFD show that there is no detectable (within the bounds of experimental/numerical accuracy) effect of the passive air jets.

It was originally expected that the significant change in surface geometry caused by the introduction of such a passive jet so close to the leading edge might result in a disturbance of the leading-edge suction and a significant boundary-layer displacement effect and thereby drag increase. This, however, does not appear to be the case. The experimentally measured drag coefficient at low angles of attack (via the Jones [18] method) was not found to be significantly different with or without the passive air jet. The CFD solutions predicted only a very small (less than 2%) increase in C_A at low angles of attack. It must be noted, however, that for moderate-to-high angles of attack (greater than 5 deg), the Spalart–Allmaras turbulence model gave progressively poorer values of C_D when compared with the experimentally derived figures. This can be explained by the experimental deficiencies of the Jones method and known inadequacies of the turbulence model for highly separated flows.

The passive air jets were found to increase maximum C_N by 14% over that achieved by the baseline model and to delay the onset of trailing-edge separation by $\Delta\alpha \sim 2$ deg. The occurrence of stall, indicated by maximum C_N, was delayed from $\alpha = 15$–16 to 18–

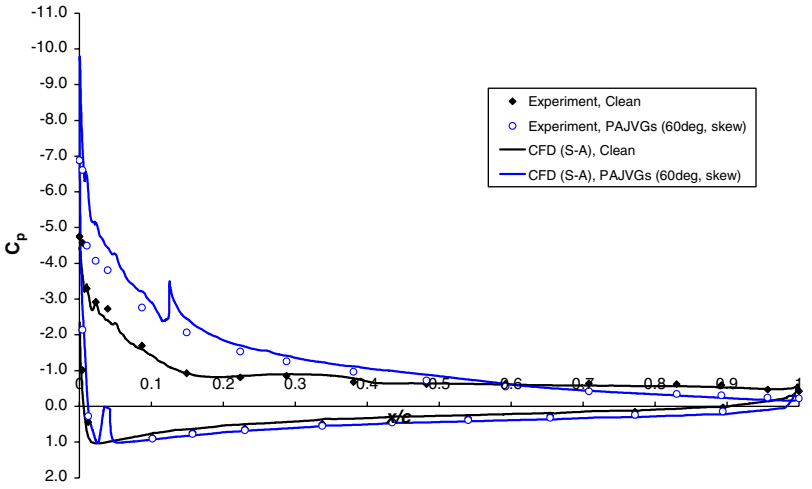

a) Jet exit center plane, y = 22.5mm

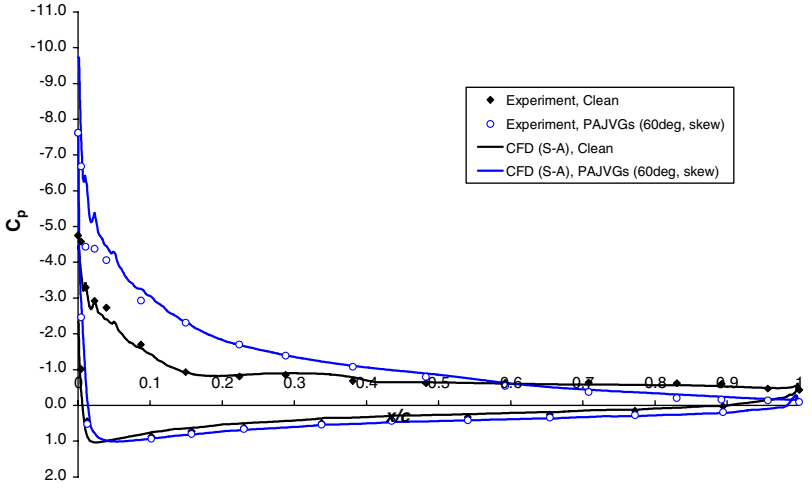

b) Midjet plane, y = 0mm

Fig. 8 Comparison of experimentally measured and CFD predicted Surface C_p distributions for the NACA 23012C model; $U = 35$ m/s, $Re_C = 1.1 \times 10^6$, and $\alpha = 18$ deg.

19 deg by the action of passive air jets, and pitching moment stall was similarly seen to be delayed by $\Delta\alpha \sim 2$ deg. Between $\alpha =$ 14–22 deg, passive air jets were found to have significantly increased C_N and negative C_A (indicative of the strength of leading-edge suction), with a significantly lower nose-up pitching moment. These effects are the same as would be expected of actively blown air jets operating at the same average C_μ, but they are achieved by a natural process with no active energy input.

The CFD study indicated (Fig. 5) that the passive air jet set at a 30 deg skew angle was not quite as effective as with 60 deg skew. This agrees with the findings of Freestone [4], though there will almost certainly be a strong effect of the duct geometry inherent in this result.

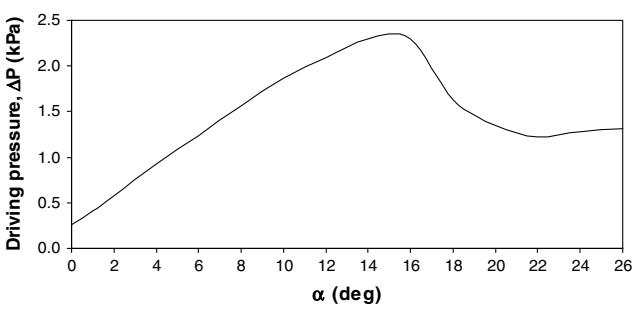

Fig. 9 Estimated driving pressure for the passive AJVG system on the NACA 23012C model at $U = 35$ m/s and $Re_C = 1.1 \times 10^6$.

An experimental survey of the upper-surface boundary layer was performed to confirm that passive air jets are, indeed, generating the classic boundary-layer embedded streamwise vortices, responsible for enhanced boundary-layer mixing and reenergization. Figure 6, comparing the experimental measurements with the corresponding N-S Spalart–Allmaras solutions, shows that the passive air jets in this $U = 35$ m/s and $\alpha = 18$ deg case do successfully generate the streamwise vortices. It is also noted that the agreement between the experimental measurements and the CFD prediction is remarkably good at all three chordwise locations, including the spatial location and structure of the vortices, though they are predicted to be slightly larger and the inner region of the boundary layer is predicted to be significantly thinner.

Interrogation of the CFD results to reveal the flow structure for the clean-airfoil and the 30- and 60-deg-skewed passive air-jet cases (Fig. 7) shows that at $\alpha = 18$ deg, the upper-surface boundary layer separates at $x/c = 0.09$ without flow control. Only a very small patch of residual leading-edge suction is evident. With passive air jets, the separation location in the midjet plane was maintained considerably further downstream in both cases, as well as lengthy regions of strong leading-edge suction. The size of the viscous wake is also seen to be considerably reduced by the action of the passive air jets. Analysis of the CFD solutions for the 30 and 60 deg skews indicate that the spanwise separation line on the upper-surface (assuming steady

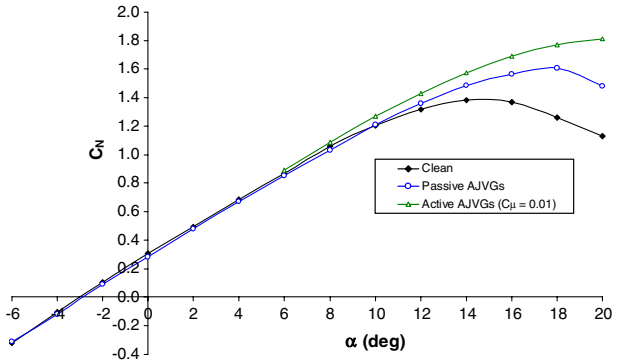

a) Normal force coefficient

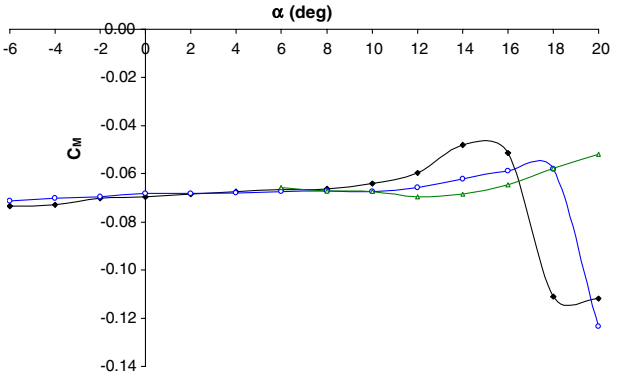

b) Quarter-chord pitching moment coefficient

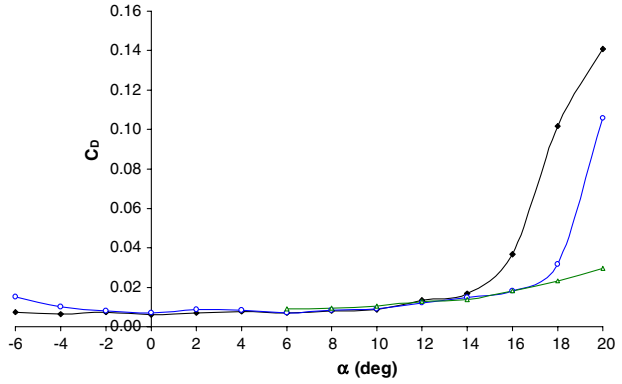

c) Drag coefficient (neglecting skin friction)

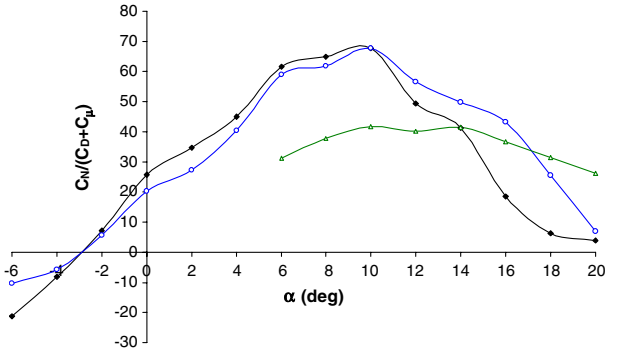

d) $C_N/(C_D+C_\mu)$

Fig. 10 Comparison of the experimentally measured aerodynamic characteristics of the NACA 23012C airfoil model with active and passive air-jet blowing; $U = 35$ m/s and $Re_C = 1.1 \times 10^6$.

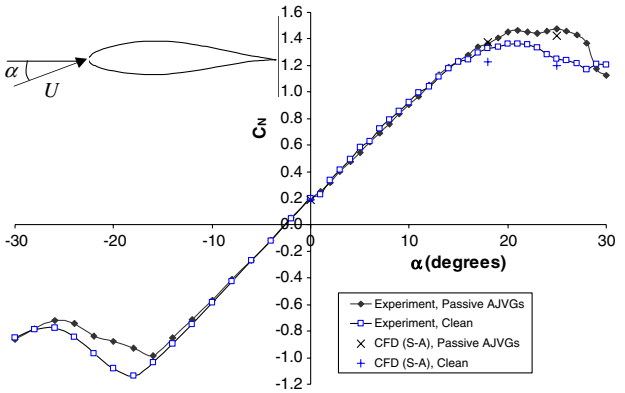

a) Normal force coefficient

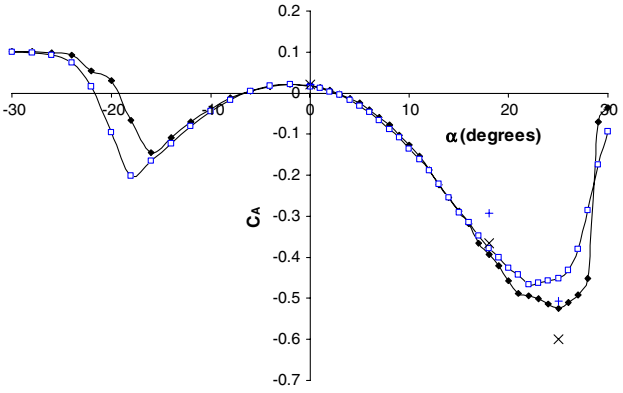

b) Axial force coefficient (neglecting skin friction)

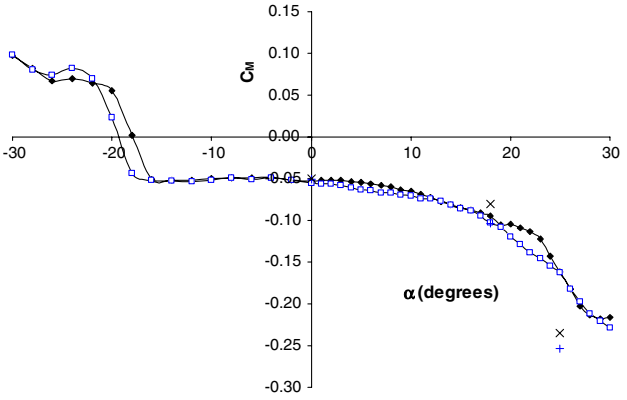

c) Quarter-chord pitching moment coefficient

Fig. 11 Comparison of the aerodynamic characteristics of the NACA 63_2-217 airfoil model with and without passive air-jet blowing; $U = 25$ m/s and $Re_C = 1.3 \times 10^6$.

Table 2 Measured drag coefficient (neglecting skin friction) for the NACA $63_2 - 217$ model with and without passive AJVGs

	Drag coefficient C_D ($\Delta C_D \sim \pm 0.002$ repeatability)	
α	Clean	Passive AJVGs
0 deg	0.010	0.009
22 deg	0.108	0.103

equilibrium), which is not presented in the figures, is wavier in appearance for the 60-deg-skew case than it is with 30 deg skew.

The comparisons of the surface pressure distributions for the clean-airfoil at $\alpha = 18$ deg and with 60-deg-skewed passive air jets are plotted in Fig. 8. Again, it can be said that there is a good agreement between experiment and CFD. It should be noted that in the jet-exit center-plane pressure distribution, the spikes in the CFD curve are the surface pressures on the air-jet intake and duct surfaces that intersect this plane. The effect of the passive air jets in maintaining the high levels of leading-edge suction is clearly evident in this data.

An important factor in the design of a passive AJVG system is obviously the pressure difference between the air-jet contoured intake and exit, which drives the flow through the duct and the attainable jet mass flow and jet-to-freestream velocity ratio. The result plotted in Fig. 9 shows that at $\alpha = 0$ deg the driving pressure difference is minimal and explains why there does not appear to be any detrimental effects on forces and moments or the pressure distribution at low angle of attack. With increasing angle of attack, up to a maximum at $\alpha = 15$–16 deg, the driving pressure difference increases almost linearly. This is exactly what is required. At zero-to-low angles of attack when there is no trailing-edge flow separation, air-jet blowing is not needed and, in fact, might be detrimental because of the boundary-layer displacement effect that might result. As trailing-edge separation approaches, however, increasing amounts of air-jet blowing are required to reenergize the upper-surface boundary layer and suppress flow separation. Strong levels of blowing will also be required once trailing-edge separation has occurred, to prevent the upstream advance of that separation front and thereby protect leading-edge suction. This is exactly the natural behavior of passive air-jet blowing, because the driving pressure difference reaches a maximum just after trailing-edge separation for the present case of the NACA 23012C model.

This is a major advantage of passive air-jet blowing, and the careful designer armed with clean-airfoil pressure data should be able to design a passive AJVG system with natural self-regulating flow behavior, such that minimal blowing occurs at low incidence and maximum blowing occurs around trailing-edge separation for the unblown airfoil.

The comparison between the effect of active blowing at $C_\mu = 0.01$ and of passive blowing on the aerodynamic characteristics of the NACA 23012C model at $U = 35$ m/s is presented in Fig. 10, and Table 3 compares the corresponding estimates of the jet-to-freestream velocity ratio (VR) and C_μ based on both experimental and CFD results, as well as the percentage changes in maximum normal force and delay in the stall angle of attack.

Although the passive AJVG system with either skew angle can only deliver C_μ of up to 0.0025 and a VR up to $\sim$1.25, the results show that the aerodynamic enhancement, although less than that achieved with $C_\mu = 0.01$ active blowing, is still significant and worthwhile. Active blowing delivered a 28% increase in maximum C_N, compared with the passive blowing result of 14%. With passive air-jet blowing, the pitching moment divergence was delayed by 2 deg (until $\alpha = 18$ deg), whereas active blowing suppressed the advent of pitching moment divergence altogether in the range (up to $\alpha = 20$ deg) investigated. The drag divergence begins at around $\alpha = 14$ deg for the clean-airfoil: 2 deg above the incipient trailing-edge angle of attack. Passive air-jet blowing delayed the drag rise until between 17 and 18 deg: 3–4 deg beyond the onset of trailing-edge separation. Active blowing at VR = 2.5 ($C_\mu = 0.01$), however, completely suppressed the drag rise in the $\alpha = 0$–20 deg range. The final plot of Fig. 10 presents the variation of the effective lift-to-drag coefficient, $C_L/(C_D + C_\mu)$, with angle of attack. The lift-to-drag ratio for the clean model and the passive air-jet cases appear to be equivalent, within the limits of experimental accuracy, up to $\alpha = 10$ deg. Beyond this angle of attack, the data show that passive air-jet blowing gives increasingly higher lift-to-drag ratios than the equivalent clean-airfoil case. Because the effective lift-to-drag ratio includes the effect of air-jet blowing momentum coefficient, the data show that active air-jet blowing at $C_\mu = 0.01$ gives significantly reduced effective lift-to-drag ratio performance except at the highest angles of attack. This graph most effectively illustrates the relative efficiency of passive air-jet blowing and the relative inefficiency of active air-jet blowing.

Table 3 Performance comparison of active and passive AJVGs on NACA 23012C model

Air-jet blowing	Active	Passive	Passive
Skew angle, deg	60	30	60
Velocity ratio	2.50	1.25	1.27
C_μ	0.0100	0.0024	0.0025
ΔC_N, %	28	9	14
$\Delta\alpha_{stall}$, deg	5	3	3

B. Passive AJVG Blowing on the NACA 63_2-217 Model

The grid sensitivity study performed for this case resulted in the same finding as with the NACA 23012C study, whereby the 2-million-cell grid solutions were confirmed to be grid-independent when compared with a 1.6-million-cell grid solution.

The comparison of the $U = 25$ m/s experimental results for the NACA 63_2-217 model, presented in Fig. 11, reveals that passive air jets have an enhancement effect on the aerodynamic characteristics on this thicker airfoil-section model that is similar to that on the more slender NACA 23012C model. In this case, the passive AJVGs increased maximum C_N by $\sim$9%, whereas the moment divergence was delayed by $\Delta\alpha \sim 2$–3 deg. The maximum axial force increased by $\sim$12% with the action of passive air-jet blowing.

Table 2 shows that, within the accuracy of the experimental instrumentation and numerical integration routine, there did not seem to be any appreciable affect of passive air-jet blowing on the drag coefficient at the two angles of attack at which this was measured. This would tend to infer that there would not be any significant improvement in the lift-to-drag ratio until above $\alpha = 16$ deg, where the increase is derived from the increase in lift coefficient due to the action of the passive air jets.

The results of the CFD study verified these findings, in that they exhibited the same trends in $C_{N\max}$ and $C_{A\max}$ and the delay in pitching moment divergence. The agreement between the experimental measurements and the CFD solutions were good enough to be confident that the numerical results resolved the correct physical affect of the air jets on the flowfield. For the $\alpha = 25$ deg case, the clean-airfoil solution was not found to converge, indicating that the flow was likely to be highly separated and therefore unsteady in nature. After running the calculation in time-accurate mode, with a maximum of 50 iterations for each 1 ms time step, the solution stabilized to predict a periodic ($\sim$12 Hz) unsteady flow whereby the leading edge was fully separated and large-scale eddies were resolved, being periodically shed from the leading edge. The force and moment data for the clean-surface case at $\alpha = 25$ deg, plotted in Fig. 11, are therefore the time-averaged results. The equivalent steady-state CFD calculation for the passive AJVG case converged well, indicating no resolution of large-scale flow unsteadiness.

Interrogation of the CFD solutions for $\alpha = 18$ and 25 deg on the spanwise planes cutting through the air-jet exit center and midway between jet centers (Fig. 12) reveals that the passive air jets act to suppress leading-edge separation and defend leading-edge suction in the same manner as predicted in the NACA 23012C calculations. At $\alpha = 18$ deg, the numerical predictions indicate that passive air jets are able to suppress the advance of the separation front, thereby reducing the viscous wake and maintaining higher levels of leading-

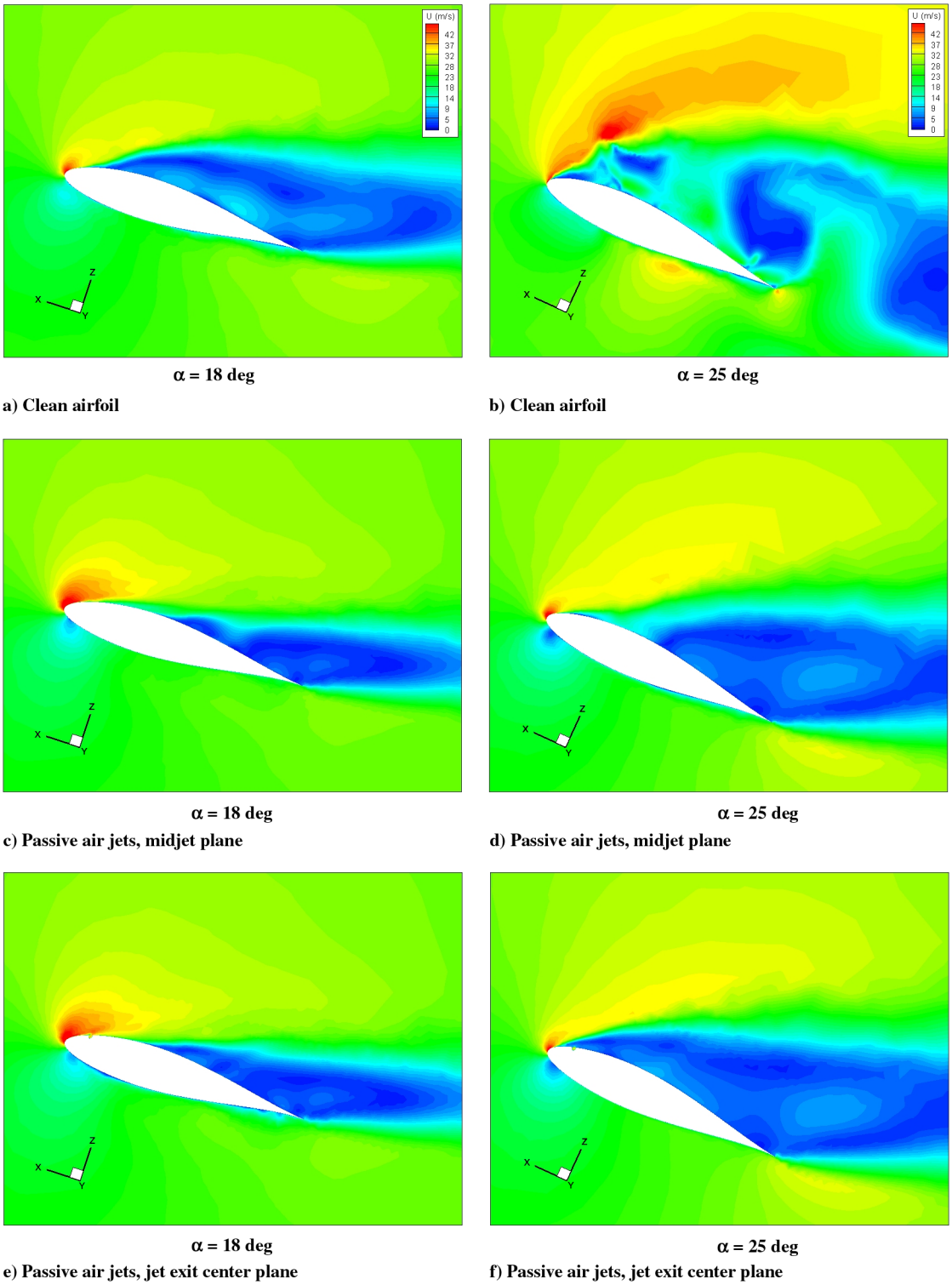

α = 18 deg
a) Clean airfoil

α = 25 deg
b) Clean airfoil

α = 18 deg
c) Passive air jets, midjet plane

α = 25 deg
d) Passive air jets, midjet plane

α = 18 deg
e) Passive air jets, jet exit center plane

α = 25 deg
f) Passive air jets, jet exit center plane

Fig. 12 Comparison of computed velocity contours at spanwise slices midway between the passive air-jet exit centers and through the passive air jet center, for the NACA 63_2-217 airfoil with and without passive air jets; $U = 25$ m/s, $Re_C = 1.3 \times 10^6$, and $\alpha = 18$ and 25 deg.

edge suction. For $\alpha = 25$ deg, the plot of the computed velocity contours for the clean-surface case (Fig. 12b) was chosen for a case in which the normal force corresponded with its average level in its cycle. From this plot, it is clear that the N-S Spalart–Allmaras solution predicts a deep-stall situation with large-eddy shedding from the leading edge of the NACA 63_2-217 sectioned model. The CFD results predict that the passive air jets act to maintain attached flow on the leading 5% chord of the upper surface, thereby maintaining residual leading-edge suction and delaying the onset of unsteady deep stall.

VI. Conclusions

The results of the experimental tests of the passive air-jet vortex generator on both a NACA 23012C and a NACA 63_2-217 airfoil-section model and the corresponding Navier–Stokes CFD calculations have confirmed that a spanwise array of passive air-jet vortex generators can effectively delay trailing-edge separation and subsequent stall to higher angles of attack, thereby increasing maximum C_N, C_L, and C_L/C_D and delaying drag and pitching moment divergence. This study has shown that the passive AJVG,

making use of a purely natural process, can achieve worthwhile aerodynamic performance improvements for airfoil-sectioned elements, such as aircraft wings and helicopter or wind turbine rotor blades, without the need for any active energy input and without significant drag penalty.

Acknowledgments

This work was supported and funded by the U.K. Ministry of Defence, Department of Trade and Industry, Augusta-Westland, Ltd., and QinetiQ, Ltd. The authors thank Sunil Mour, Vital Gutierrez, Chris Barber, Tim Barnes, and Mike Smith for their contributions to this work.

References

[1] Taylor H. D., and Hoadley, H. H., "Application of Vortex Generator Mixing Principle to Diffusers," United Aircraft Corp., Rept. R-15064-5, East Hartford, CT, 1948.

[2] Wallis, R. A., "The Use of Air Jets for Boundary Layer Control," Aeronautical Research Labs., Rept. 110, Melbourne, Australia, 1952.

[3] Pearcey, H. H., "Shock Induced Separation and Its Prevention by Design and Boundary Layer Control," *Boundary Layer and Flow Control*, edited by G. V. Lachmann, Pergamon, New York, 1961, pp. 1166–1134.

[4] Freestone, M., "Preliminary Tests at Low Speeds on the Vorticity Produced by Air-Jet Vortex Generators," City Univ., Rept. 85/1, London, 1985.

[5] Johnston J. P., and Nishi, M., "Vortex Generator Jets—A Means of Flow Separation Control," AIAA Paper 89-0564, 1989.

[6] Compton D. A., and Johnston, J. P., "Streamwise Vortex Production by Pitched and Skewed Jets in a Turbulent Boundary Layer" *AIAA Journal*, Vol. 30, No. 3, 1992, pp. 640–647. doi:10.2514/3.10967

[7] Selby, G. V., Lin J. C., and Howard, F. G., "Control of Low Speed Turbulent Separated Flow Using Jet Vortex Generators," *Experiments in Fluids*, Vol. 12, No. 6, 1992, pp. 394–400.

[8] Innes, F., Pearcey, H. H., and Sykes, D. M., "Improvements in the Performance of a Three Element High Lift System by the Application of Air Jet Vortex Generators," *Aeronautical Journal*, Vol. 99, No. 4, 1995, pp. 265–274.

[9] Oliver, A. G., "Air Jet Vortex Generators for Wind Turbines," Ph.D. Dissertation, City Univ., London, 1997.

[10] Raghunathan, S., Watterson, J. K., Cooper, R. K., and Kelly, B., "A Novel Concept of Passive Vortex Generator Jets for Separation Control," AIAA Paper 99-1004, 1999.

[11] Singh, C., Peake, D. J., Coton, F., Kokkalis, A., Khodagolian, V., and Galbraith, R. A., "Parametric Study of an Air-Jet Vortex Generator Configuration to Control Rotorcraft Retreating Blade Stall," 43rd AIAA Aerospace Sciences Meeting and Exhibit, Reno, NV, AIAA Paper 2005-1366, Jan. 2005.

[12] Singh, C., "Application of Air Jet Vortex Generators to Control Helicopter Retreating Blade Stall," Ph.D. Dissertation, City Univ., London, 2007.

[13] Singh, C., and Prince, S. A., "Report on experimental activities for AJVG's," *Rotorcraft Aeromechanics DARP Programme*, Augusta-Westland, Ltd., Rept. D1.2, Yeovil, Somerset, England, U.K., Apr. 2004.

[14] Prince, S. A., "An Experimental and Computational Assessment of Passive Air Jet Flow Control for Stall Suppression at Low Speed," *Rotorcraft Aeromechanics DARP Programme*, Augusta-Westland, Ltd., Rept. D1.8b, Yeovil, Somerset, England, U.K., May 2007.

[15] Prince, S. A., Khodagolian, V., Singh, C., Mour, S., and Kokkalis, A., "Aerodynamic Stall Suppression on Aerofoil Sections Using Passive Air Jet Vortex Generators, Anchorage, Alaska," International Council of the Aeronautical Sciences Paper 2008-3.11.3, Sept. 2008.

[16] Krzysiak, A., "Control of Flow Separation Using Self-Supplying Air-Jet Vortex Generators," *AIAA Journal*, Vol. 46, No. 9, 2008, pp. 2229–2234. doi:10.2514/1.30150

[17] Green, R. B., and Galbraith, R. A. M., "Dynamic Recovery to Fully Attached Airfoil Flow from Deep Stall," *AIAA Journal*, Vol. 33, No. 8, 1995, pp. 1433–1440. doi:10.2514/3.12565

[18] Jones, B. M., "The Measurement of Profile Drag by the Pitot-Traverse Method," Aeronautical Research Council Reports and Memoranda No. 1688, London, Jan. 1936.

[19] FLUENT, Software Package, Ver. 6, ANSYS, Inc., Canonsburg, PA, 2005.

[20] Spalart, P., and Allmaras, S.. "A One-Equation Turbulence Model for Aerodynamic Flows," AIAA Paper 92-0439, 1992.

[21] Launder, B. E., and Spalding, D. B., "Lectures in Mathematical Models of Turbulence," Academic Press, London, 1972.

[22] Menter, F. R., "Two-Equation Eddy-Viscosity Turbulence Models for Engineering Applications," *AIAA Journal*, Vol. 32, No. 8, 1994, pp. 1598–1605. doi:10.2514/3.12149

F. Coton
Associate Editor